Geophysical Prospecting

EAGE EUROPEAN ASSOCIATION OF GEOSCIENTISTS & ENGINEERS

Geophysical Prospecting, 2011, **59**, 1035–1045 doi: 10.1111/j.1365-2478.2011.01007.x

Scalar, vector, tensor magnetic anomalies: measurement or computation?

Marc Munschy* and Simon Fleury

Institut de Physique du Globe de Strasbourg, Université de Strasbourg / EOST, CNRS, 1, rue Blessig, CS90032, 67081 Strasbourg Cedex, France

Received January 2011, revision accepted August 2011

ABSTRACT

Magnetic surveys for geophysical interpretation will most usefully furnish estimates of the three components of the magnetic field vector. We review methods for obtaining this information based on scalar and tensor magnetic field measurements and point out the advantages of fluxgate vector measurements. Fluxgate vector magnetometers can be powerful instruments in magnetic mapping. The main problems in using fluxgate magnetometers arise from calibration errors and drift but these can be overcome using a quick and simple method of calibration. This method also has the advantage of compensating permanent and induced magnetic fields generated by the airplane. This is illustrated by a new aeromagnetic survey flown in the Vosges area (France). Measurement accuracy is shown to be similar to that obtained with scalar magnetometers. We take advantage of this accuracy to calculate in the Fourier domain other magnetic functions from the total-field anomaly, in particular, the magnetic gradient tensor is obtained without using any superconducting quantum devices. A similar approach is used to introduce a new magnetic anomaly tensor that is the equivalent of the pseudo-gravity tensor. Maps presented in the last sections serve as an example to illustrate the various functions, the goal of the paper being to obtain magnetic vector data from the observations without first postulating the detailed nature of the sources.

Key words: Airborne, Fluxgate magnetometer, Magnetic, Magnetic anomaly, Magnetic data transformations.

INTRODUCTION

Magnetic field measurements for exploration can be acquired either using land, airborne, marine, space or down borehole platforms. Depending on the purposes of the study, various magnetic functions may be measured ranging from scalar or vector anomaly to gradient of the magnetic field or gradient tensor anomaly. The preliminary sections serve as a review to evoke how these various magnetic functions are assessed by relevant magnetic equipment.

*E-mail: marc.munschy@unistra.fr

SCALAR MAGNETOMETRY

Airborne magnetic surveys are most often performed with scalar magnetometers with sensitivities around 0.01 nT and sample rates of 1–10 Hz. Alkali magnetometers (Hardwick 1984a) are mainly used but proton or overhauser magnetometers (Abragam 1961) are still in use. The difficulty for airborne magnetic surveying is to accurately remove the magnetic effect of the airplane. A mathematical solution was brought by Leliak (1961) and Leach (1980) using the measurement of the three components of the total magnetic field in the frame of the airplane. The compensation algorithm is based on linear regression of parameters corresponding to

permanent (three parameters) and induced (six parameters) magnetic fields.

Permanent magnetic fields do not vary with the movements of the sensor and can be expressed at the sensor's orthonormal coordinate system as a constant vector. Induced magnetic fields vary with the orientation of the sensor because magnetizations remain parallel to the Earth's magnetic field. So, the only cause of variation of the induced magnetic field at the sensor's orthonormal coordinate system is the attitude of the sensor. Leliak (1961) and Leach (1980) showed that the induced magnetic field can be expressed at the sensor's orthonormal coordinate system by a lower triangular matrix containing six unknowns.

Magnetic fields from eddy-currents are the third source of interference in aeromagnetic measurements. These magnetic fields are proportional to changes over time in the flux of the Earth's magnetic field through induction from elements of the measuring system. Their effect may be written in the same manner as those of the permanent and induced field expressions.

VECTOR MAGNETOMETRY

Vector fluxgate magnetometers (Primdahl 1979) allow direct measurement of the magnetic field components. They have several important advantages for magnetic mapping such as cost, size, low power requirements and high sampling rate. However they are less commonly used because they are not absolute instruments and are less accurate with a sensitivity of about 1 nT. Moreover, in practice, there are no sensors available so far allowing accurate measurements of the three magnetic field components with respect to an Earth's coordinate system. This is why, such magnetometers have to be calibrated in order to produce acceptable measurements: changing the attitude of the magnetometer in an area where the intensity of the magnetic field is constant gives a variation of the measured intensity of generally more than 100 nT, which is unacceptable for magnetic mapping. An elegant solution to this problem was proposed by groups working on the calibration of vector magnetometers on satellites (e.g., Marklund, Blomberg and Persson 2001; Sabaka, Olsen and Purucker 2004). The problem is solved mathematically using two presuppositions: 1) the magnetometer is rotated in all directions in an area where the intensity of the magnetic field is known and 2) the magnetometer errors are then the only cause of discrepancy between the actual and measured intensities of the magnetic field. For a particular magnetic measurement, the magnetometer output $\mathbf{F} = (F_1, F_2, F_3)$ is connected to the magnetic field $\mathbf{B} = (B_1, B_2, B_3)$ according to $F = \mathbf{S} \bullet \mathbf{P} \bullet \mathbf{B} + \mathbf{O}$, where $\mathbf{O} = (o_1, o_2, o_3)$ is the offset vector and $\mathbf{S}$ is the diagonal matrix of sensitivities,

$$S = \begin{bmatrix} s_1 & 0 & 0 \\ 0 & s_2 & 0 \\ 0 & 0 & s_3 \end{bmatrix},$$

$\mathbf{P}$ is the 3×3 matrix, which transforms a vector from the orthogonal magnetic axes coordinate system to the sensor axes coordinate system,

$$\mathbf{P} = \begin{bmatrix} 1 & 0 & 0 \\ -\sin u_1 & \cos u_1 & 0 \\ \sin u_2 & \sin u_3 & \sqrt{1 - \sin^2 u_2 - \sin^2 u_3} \end{bmatrix},$$

with u_1, u_2 and u_3 the three non-orthogonality angles assumed close to zero (Olsen *et al.* 2001). Then the mathematical model of magnetometer errors contains nine parameters: three offset errors, three sensitivity errors and three non-orthogonality angles. To estimate the nine parameters, a linearized least-square approach of the model parameters can be used (Olsen *et al.* 2001). This is called a scalar calibration because only the intensity of the magnetic field is used. It is different to a vector calibration where the output of the vector magnetometer is compared with the magnetic field vector (Olsen *et al.* 2001). Such a procedure was applied to a fluxgate magnetometer (Munschy *et al.* 2007) to obtain scalar magnetic anomalies. In a signal range of about 220 nT for the magnetic field, the pre-calibration standard deviation was 63.6 nT, while after calibration the standard deviation was 1.4 nT. Munschy *et al.* (2007) also showed that the compensation procedure uses the same equations as the calibration procedure, the induced and remanent magnetic fields produced by magnetized elements act in exactly the same way on the sensor as the nine errors of calibration. This was checked under real conditions. A piece of ferrous material was attached to the fluxgate magnetometer. The pre-calibration standard deviation was 520 nT, while after calibration the standard deviation was 1.9 nT. Therefore the method of calibrating fluxgate magnetometers proposed correctly not only the limitations of the magnetometer but also the remanent and induced fields from other equipment carried with the sensor. These corrections of perturbating magnetic fields cannot be performed with scalar sensors because the method requires the measurement of the three components of the magnetic field.

After calibration the remaining signal corresponds to the noise of the sensor and of the analogue-digital converter. The histogram of this signal in the case described above is of a Gaussian form with a standard deviation of 1.4 nT.

It is difficult to know if the noise is due primarily to the sensor, which has a standard internal noise of 0.1 nT or to the A/D sigma delta converter that has a dynamics range of 19 bits.

MAGNETIC GRADIOMETRY AND TENSOR MEASUREMENTS

There are several advantages to measure gradients of the magnetic field instead of the vector field itself (Hardwick 1984b). The signal varies much less than the vector signal and it is less sensitive to manoeuvres of the airplane; it does not contain temporal variations; it better resolves the anomalies. Many aeromagnetic surveys use several scalar magnetometers to obtain one or several gradients and more often the vertical gradient is measured.

Superconducting quantum interference devices allow measurements of the magnetic tensor with sensitivity on the order of 10^{-4} nT.m^{-1} (Schmidt and Clark 1998; Stolz *et al.* 2006; Fitzgerald *et al.* 2010). Such magnetometers, using superconducting properties, present some difficulties, in particular the complex logistics for cryogens and associated systems. Also, the compensation of the magnetic effect of the airplane remains a problem (Hardwick 1984b; Fitzgerald and Holstein 2006) and it cannot be orientated precisely in an Earth's coordinate system. These difficulties of implementation reduce the progression of this equipment.

From a theoretical point of view, a vector is associated with possible derivatives, each component of the vector being derived along three orthogonal axes, which form the gradient tensor (Nelson 1988; Schmidt and Clark 1998).

AN EXAMPLE OF AN AEROMAGNETIC SURVEY WITH A VECTOR SENSOR

The aeromagnetic map (Fig. 1) was obtained by using two fluxgate magnetometers installed in the wing tips of a Maule MX7 airplane and no compensation equipment or software was used. The area surveyed is located in Vosges, France (48°14'– 48°25'N and 6°50'– 7°11'E) and represents an area of 20 × 30 km flown at an altitude of 900 m above sea level with a line spacing equal to 500 m. East-west tie lines have a spacing of 2–3 km. Magnetic data are sampled at a rate of 30 Hz. This sampling rate and the line spacing provide a high-resolution acquisition and prevent aliasing. Before and after each flight, a calibration is performed, the airplane drawing an eight-shaped figure about 2 km wide. The calibration procedure was tested by performing an eight-shaped pattern in which the aircraft undergoes a sequence of yaw, pitch and roll manoeuvres at an altitude of 500 m above the ground surface, over a magnetically quiet area. The pre-calibration standard deviation was 440 nT, while after calibration the standard deviation was 1.9 nT (Fig. 2). Flight data are corrected using the calibration parameters and the intensity of the magnetic field is computed. Standard procedures are used to compute a magnetic anomaly grid with a cell-size of 100 m: verification and edition of the raw data, removing temporal variation, removing of the International Geomagnetic Reference Field (Finlay *et al.* 2010) and computation of the grid (D'Errico 2010). The data quality is checked by computing the difference of the measured magnetic field at line crossings: a standard deviation of 2.7 nT is obtained for the 446 crossing points. This value is in agreement with the results obtained after calibration.

The aeromagnetic map presented here serves as an example to illustrate the various results obtained to compute the vector magnetic field and tensors, the goal of the paper being not to propose a geological interpretation of the magnetic data.

VECTOR COMPUTATION USING MAGNETIC ANOMALY

Assuming that the magnitude of the anomalous magnetic field is small compared to the Earth's magnetic field, the scalar measurements correspond to the derivative of the magnetic potential in the direction of the Earth's magnetic field (Baranov 1957), i.e.,

$$F = -\frac{\partial U}{\partial \vec{t}}, \tag{1}$$

with U the magnetic potential, F the total-field anomaly and $\vec{t}$ a unit vector in the direction of the Earth's magnetic field. This equation is valid only if the total-field anomaly is much smaller than the Earth's magnetic field, which is generally the case. The approximation introduced by the computation depends on the inclination and the magnitude of the magnetic field. For example the error is less than 1% when the magnitude of the total-field anomaly is less than 1000 nT with an Earth's magnetic field of 50 000 nT. Lourenco and Morrison (1973) proposed an iterative method to compute the true value of the total-field anomaly even if the approximation is not valid. In the case of our aeromagnetic survey, the maximum difference is equal to 0.7 nT for maximum amplitude of 450 nT for the total-field magnetic anomaly.

Having computed the magnetic potential, the vector magnetic anomaly is obtained in the wavenumber domain using

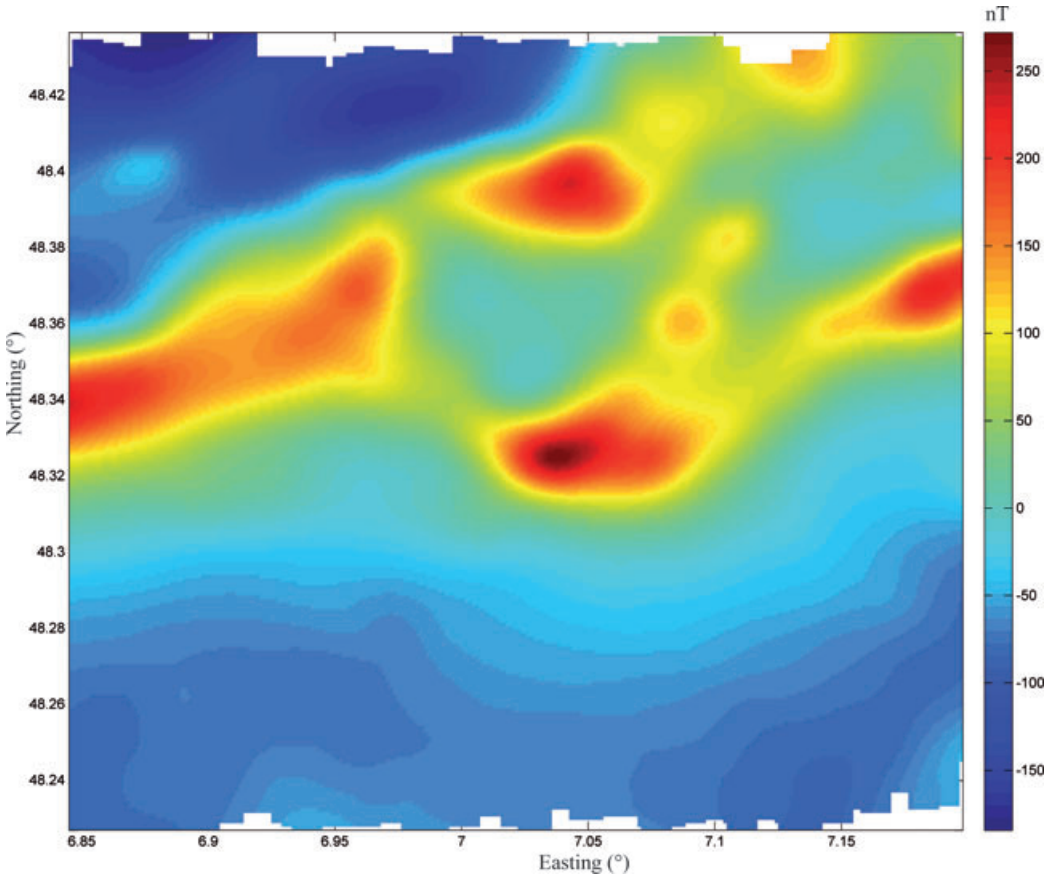

Figure 1 Total-field magnetic anomaly map of the surveyed area.

the gradient operator, i.e.,

$$\mathbf{C} = \begin{bmatrix} -iu \\ -iv \\ s \end{bmatrix} U = \begin{bmatrix} iu \\ iv \\ -s \end{bmatrix} \frac{F}{ilu + imv - ns}, \tag{2}$$

with, u and v, the wavenumbers in the horizontal directions, $s = \sqrt{u^2 + v^2}$ and (l, m, n) the coordinates of the unit vector in the direction of the regional magnetic field.

Not only the magnitude of the vector magnetic anomaly can be displayed and interpreted but also the three vector components (Fig. 3). Indeed, the reduction to the pole of the regional field applied to the total-field anomaly corresponds to the vertical derivative of the magnetic potential (Z-component, Fig. 3e). The vector magnetic anomaly can be displayed in diverse manners as vector plots (Fig. 4) or in spherical coordinates (Fig. 3f–h). Such maps show the magnetic field in diverse manners and help for a better interpretation. For example, the azimuth component of the magnetic anomaly displayed in spherical coordinates (Fig. 3) shows sharp colour variations that could correspond to the main geological contacts in the area.

COMPUTATION OF THE MAGNETIC ANOMALY TENSOR

There are several possibilities for defining a magnetic tensor. Broadening the definition (1) of Baranov (1957), let us consider the scalar magnetic potential as the derivative of a scalar function in the magnetization direction. In this case, this new function is the superpotential of the magnetic field, the equivalent of the gravimetric potential (Beiki, Pedersen and Nazi 2011). We have

$$F = \frac{\partial^2 W}{\partial t^2}, \tag{3}$$

with W the magnetic superpotential, F the total-field anomaly and t a unit vector in the direction of the Earth's magnetic field that is supposed to be parallel to the Earth's magnetic field.

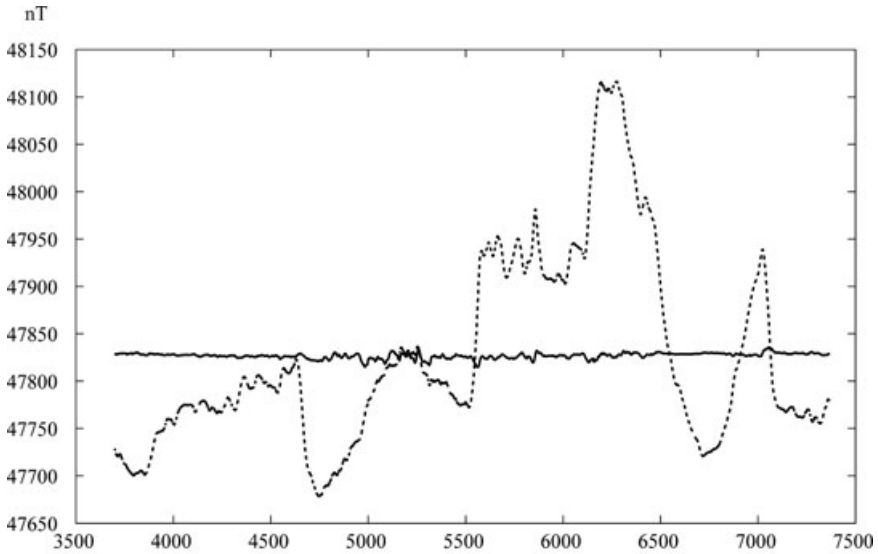

	Calibration	Offset	Non-orthogonality angle (°)
X Sonde	1.001741 (+/- 0.000070)	-474.7 (+/- 3.5)	-0.187872 (+/- 0.004035)
Y Sonde	1.001962 (+/- 0.000038)	-105.2 (+/- 1.6)	0.120143 (+/- 0.000868)
Z Sonde	1.002986 (+/- 0.000039)	84.1 (+/- 0.6)	0.038895 (+/- 0.000293)

Figure 2 Results of an in-flight calibration. The two curves correspond to the non-calibrated (dotted line, std = 102.0 nT) and calibrated (solid line, std = 2.5 nT) intensities of the magnetic field measured by the fluxgate sensor. The nine estimated calibration parameters are given at the bottom of the figure.

The magnetic anomaly tensor is computed in the frequency domain using the tensor product, i.e.,

$$\mathbf{T}_M = \begin{bmatrix} -u^2 & -uv & -ius \\ -uv & -v^2 & -ivs \\ -ius & -ivs & s^2 \end{bmatrix} W = \begin{bmatrix} -u^2 & -uv & -ius \\ -uv & -v^2 & -ivs \\ -ius & -ivs & s^2 \end{bmatrix} \frac{F}{(ilu + imv - ns)^2}. \quad (4)$$

The magnetic tensor is symmetric and its trace is equal to zero (Fig. 5). Because of its property of symmetry the tensor can be diagonalized by computing its eigenvalues and eigenvectors. Pedersen and Rasmussen (1990) studied the maximum eigenvalues and associated eigenvectors of the gravity gradient tensor related to the centre of mass for a simple point source. Figure 6 presents a magnetic anomaly tensor eigenanalysis. This new representation of the magnetic field provides no more information than is already contained in the total-field magnetic anomaly but corresponds to another view of the magnetic field that can be more practical for interpretation.

The ZZ-component of the magnetic anomaly tensor is equal to the reduction to the pole of the Earth's magnetic field and magnetization because the reduction to the pole corresponds in this case to the second vertical derivative of the superpotential. The reduction to the pole, generally used in magnetic interpretations, corresponds to the transformation of the total-field magnetic anomaly to the total-field magnetic anomaly at the North Pole where induced magnetization and ambient field are both directed vertically down.

According to equation (3), any magnetic anomaly F may be written using the superpotential W that gives in the wavenumber domain,

$$F = (ilu + imv - ns)^2 \, W, \quad (5)$$

where direction cosines l, m, n can be expressed by the inclination and declination of the magnetization or the Earth's magnetic field.

The corresponding reduction-to-the-pole operator in the wavenumber domain is given by (Gunn 1975),

$$H = \left(\frac{s}{ilu + imv - ns} \right)^2. \quad (6)$$

The difficulty in using such a transformation appears in the equatorial region. In this case, the Earth's magnetic field is almost horizontal and the second power in the denominator of equation (6) is equal to zero when $u/v = -m/l$. In presence of noise, north-south lineation artefacts appear on the transformation map (Blakely 1995, pp. 330–335). The problem is

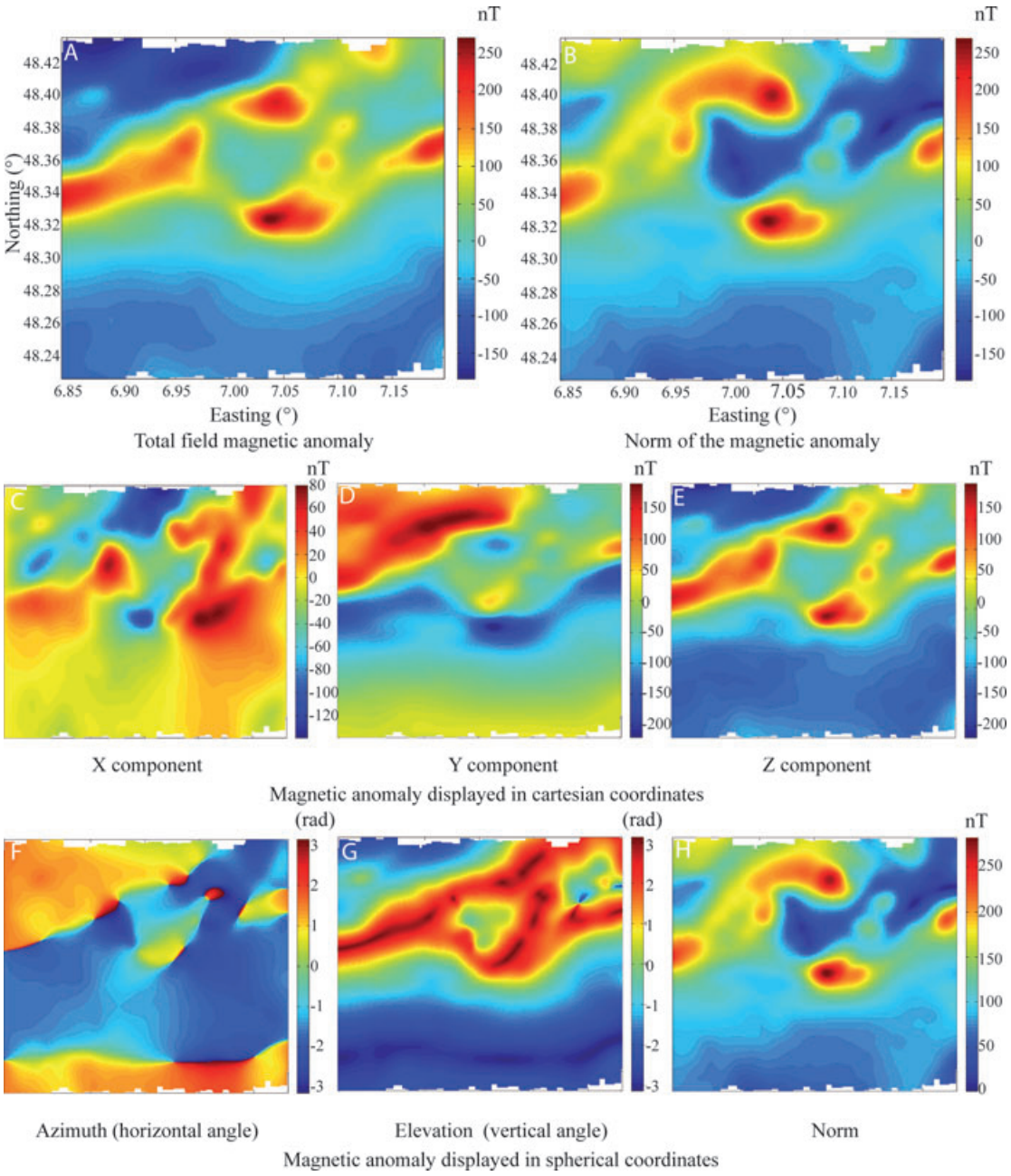

Figure 3 From top to bottom, total-field anomaly (a), magnitude of the magnetic anomaly (b), Cartesian coordinates (c–e) and spherical coordinates (f–h) of the vector magnetic anomaly. The *Z*-component (e) corresponds to the reduction to the pole of the Earth's magnetic field.

not due to a physical limitation but to a numeric instability. By calculating F_r, the magnetic anomaly reduced to the pole, one obtains,

$$F_r = s^2 W. \tag{7}$$

As W is a continuous and bounded function in a source free half-space, it follows that F_r may be computed in any case using equation (7). Therefore, there are no physical reasons that prevent from reducing to the pole any data even equatorial ones. The problem with reduction to the pole is merely due to the definition of the operator.

Magnetic gradient tensor surveys are possible since a few years (e.g., Stolz *et al.* 2006). This tensor corresponds to all the possible gradients of the magnetic field. Therefore it does

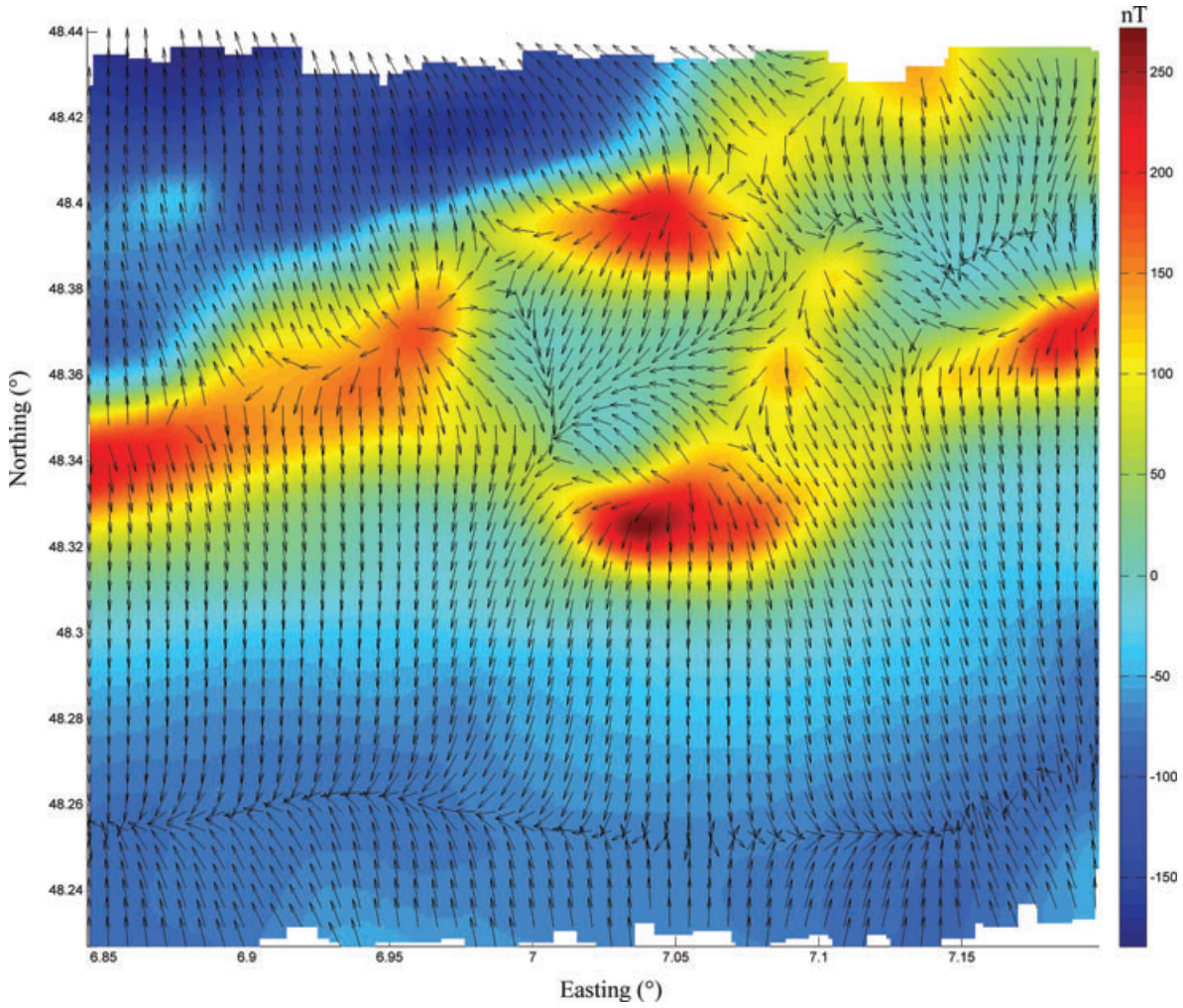

Figure 4 Total-field magnetic anomaly map of the surveyed area and arrows showing the direction of the normalized horizontal component of the magnetic anomaly field.

not correspond to the magnetic anomaly tensor described above but to the second derivatives of the magnetic potential, i.e.,

$$T_G = \begin{bmatrix} -u^2 & -uv & -ius \\ -uv & -v^2 & -ivs \\ -ius & -ivs & s^2 \end{bmatrix} U = \begin{bmatrix} -u^2 & -uv & -ius \\ -uv & -v^2 & -ivs \\ -ius & -ivs & s^2 \end{bmatrix} \frac{F}{ilu + imv - ns}. \quad (8)$$

The gradient tensor appears (Fig. 7) sharper than the anomaly tensor (Fig. 5) because it corresponds to one more order of derivation.

CONCLUSION

Scalar magnetic measurements allow the computation in the wavenumber domain of the vector magnetic anomaly or its tensor. We have described the scalar superpotential function as a new tool to derive a new magnetic anomaly tensor, relevant to magnetic interpretation. Its elements are anomaly field components produced by magnetizations directed toward each of the reference frame axis. These elements include pole and equator reductions. However, these computations have the weakness to assume the knowledge of the direction of the Earth's magnetic field for the computation of the vector magnetic anomaly and of the magnetization direction for the magnetic anomaly tensor. Also, numeric instabilities make difficult the computation of the anomaly tensor in equatorial

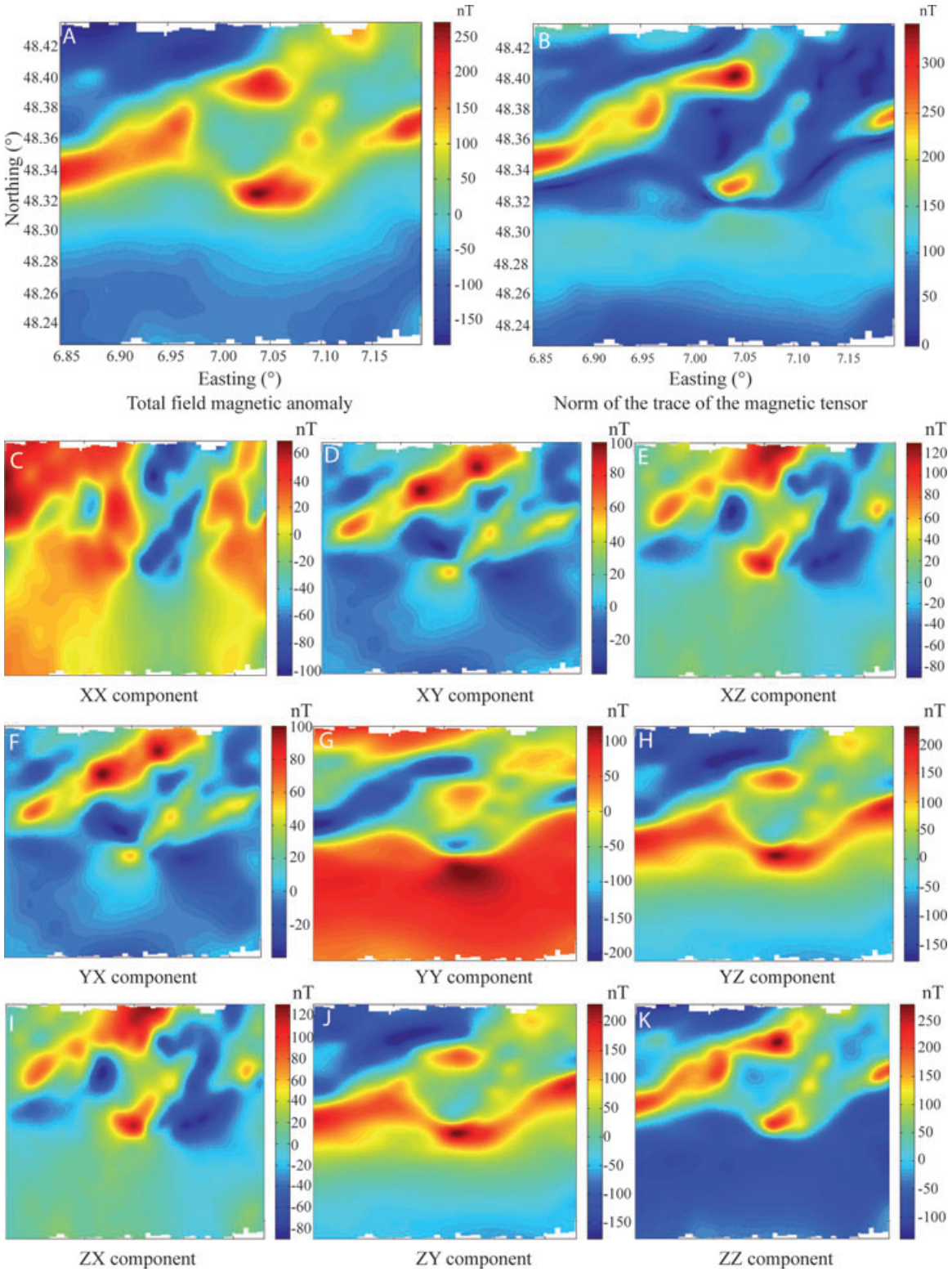

Figure 5 From top to bottom, total-field anomaly (a), norm of the trace of the magnetic anomaly tensor (b) and the nine components of the tensor displayed in matrix form (c–k). The *ZZ*-component of the tensor (k) corresponds to the reduction to the pole of the Earth's magnetic field and of the magnetization vector.

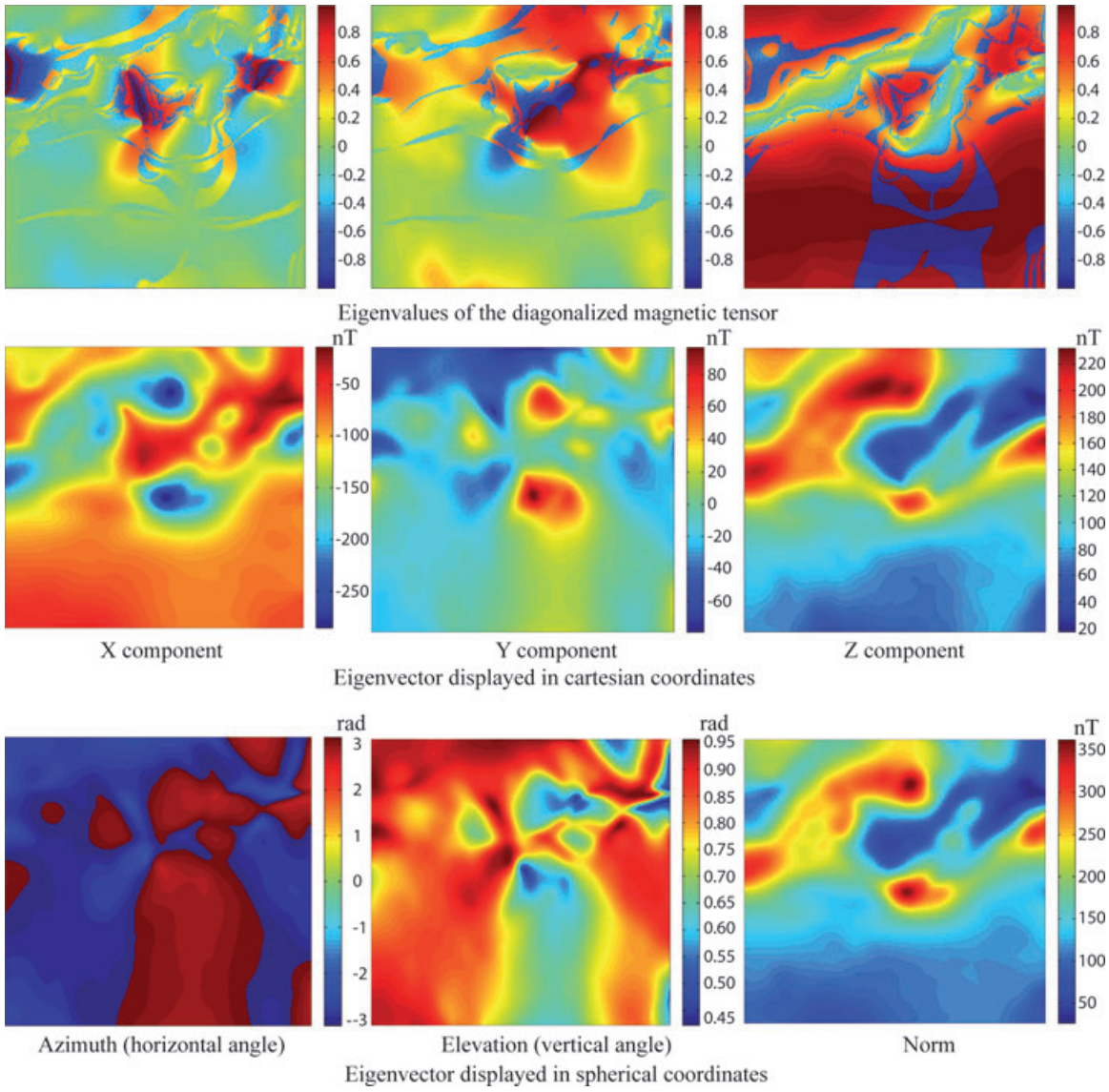

Figure 6 Representations of the diagonalized magnetic anomaly tensor. From top to bottom, eigenvalues and eigenvectors in Cartesian and spherical coordinates.

regions. It is very likely that inertial measurement units will be available soon and combined to three-component fluxgate magnetometers, measurement of the Earth's magnetic vector will be possible with sufficient accuracy. Moreover, with accurate inertial measurement equipment, a magnetic gradient tensor using superconducting magnetometers will become possible, making current limitations obsolete. Fluxgate magnetometers can already be used for magnetic mapping with an accuracy of measurements similar to that of scalar magnetometers. They have the advantage of being light and consume less power. Another advantage of fluxgate magnetometers is that the procedure of calibration also compensates for magnetic fields emanating from the airplane. Superconducting quantum interference devices also have a good potential but must overcome some difficulties of implementation.

ACKNOWLEDGEMENTS

The authors thank Editor-in-Chief Tijmen Jan Moser, Associate Editor Horst Holstein and an anonymous reviewer for their comments, which helped to improve substantially an earlier version of the paper. They would also like to thank

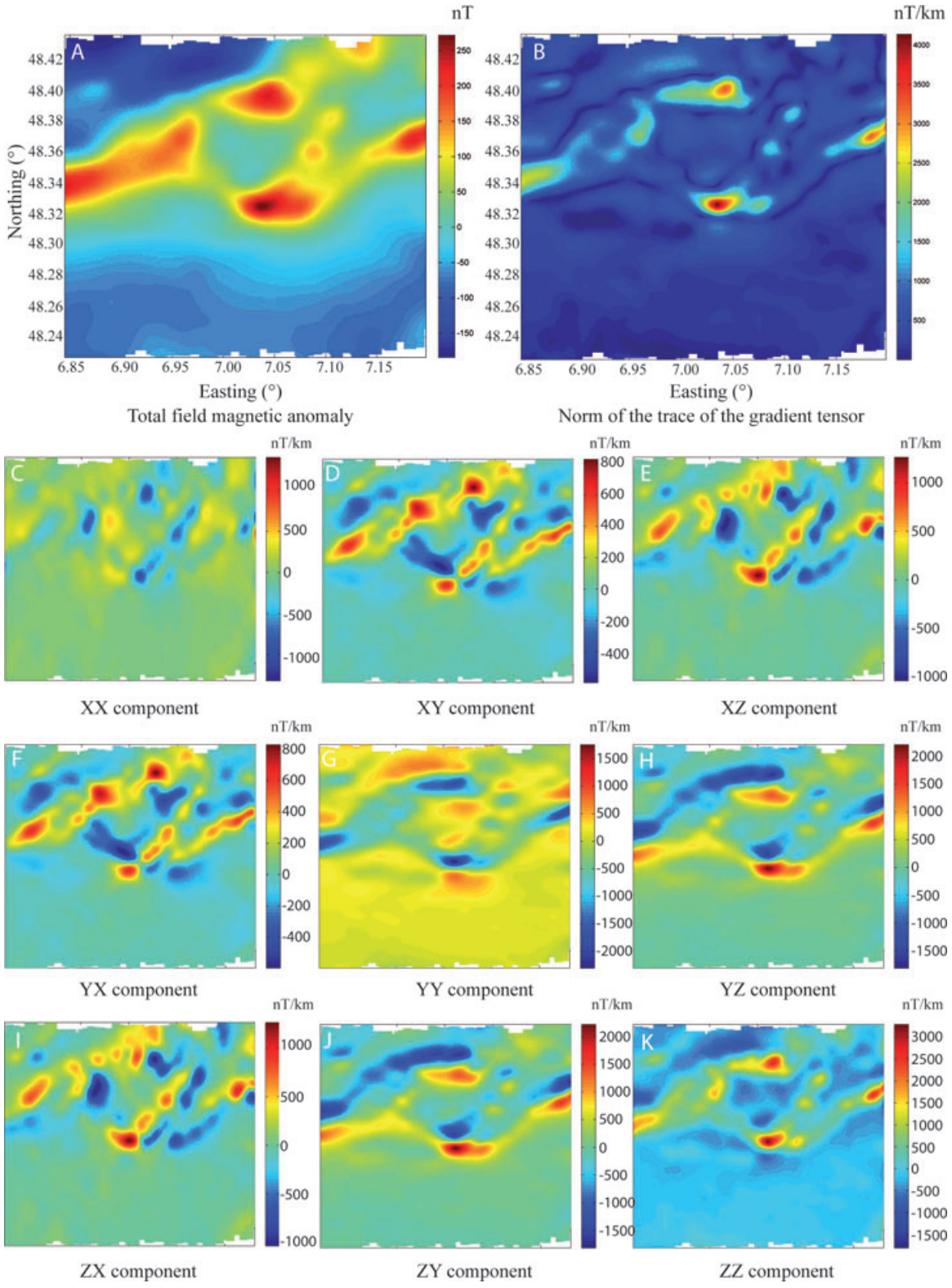

Figure 7 From top to bottom, total-field anomaly (a), norm of the trace of the magnetic gradient tensor (b) and the nine components of the tensor displayed in matrix form (c–k).

the AREVA Mining Business Group (Paris – La Défense) for financial support to Simon Fleury as a PhD student.

REFERENCES

Abragam A. 1961. *Principles of Nuclear Magnetism*. Oxford University Press. ISBN 9780198520146.

Baranov V. 1957. A new method for interpretation of aeromagnetic maps: Pseudo-gravity anomalies. *Geophysics* **22**, 359–383.

Beiki M., Pedersen L.B. and Nazi H. 2011. Interpretation of aeromagnetic data using eigenvector analysis of pseudogravity gradient tensor. *Geophysics* **76**, L1–L10.

Blakely R.J. 1995. *Potential Theory in Gravity and Magnetic Applications*. Cambridge University Press.

D'Errico J. 2010. Surface Fitting Using Gridfit. Matlab Central, the Mathworks, Inc. http://www.mathworks.com/matlabcentral/fileexchange/8998-surface-fitting-gridfit

Fitzgerald D.J., Argast D., Paterson R. and Holstein H. 2010. Full tensor magnetic gradiometry processing and interpretation developments. *EGM 2010 International Workshop Session: Advances in Instrumentation and Data Acquisition*, Expanded Abstracts.

Fitzgerald D.J. and Holstein H. 2006. Innovative data processing methods for gradient airborne geophysical data sets. *The Leading Edge* **25**, 87–94.

Finlay C.C., Maus S., Beggan C.D., Bondar T.N., Chambodut A., Chernova T.A. *et al*. 2010. International Geomagnetic Reference Field: The eleven generation. *Geophysical Journal International* **183**, 1216–1230.

Gunn P.J., 1975. Linear transformations of gravity and magnetic fields. *Geophysical Prospecting* **23**, 300–312.

Hardwick C.D. 1984a. Important design considerations for airborne magnetic gradiometers. *Geophysics* **49**, 2004–2018.

Hardwick C.D. 1984b. Non-oriented cesium sensors for airborne magnetometry and gradiometry. *Geophysics* **49**, 2024–2031.

Leach B.W. 1980. Aeromagnetic compensation as a linear regression problem. In: *Information Linkage between Applied Mathematics and Industry*, 2nd edn. (ed. A.L. Schoenstadt), pp. 139–161. Academic Press.

Leliak P. 1961. Identification and evaluation of magnetic field sources of magnetic airborne detector equipped aircraft. *Inst. Radio Eng. Trans., Aerospace Navigation Electronics* **8**, 95–105.

Lourenco J.S. and Morrison H.F. 1973. Vector magnetic anomalies derived from measurements of a single component of the field. *Geophysics* **38**, 359–368.

Marklund G.T., Blomberg L.G. and Persson S. 2001. Astrid-2, an advanced microsatellite for auroral research. *Annales Geophysicae* **19**, 589–592.

Munschy M., Boulanger D., Ulrich P. and Bouiflane M. 2007. Magnetic mapping for the detection and characterization of UXO: Use of multi-sensor fluxgate 3-axis magnetometers and methods of interpretation. *Journal of Applied Geophysics* **61**, 168–173.

Nelson J.B. 1988. Calculation of the magnetic gradient tensor from total-field gradient measurements and its application to geophysical interpretation. *Geophysics* **53**, 957–966.

Olsen N., Toffner-Clausen L., Risbo T., Brauer P., Merayo J., Primdahl F. and Sabaka T. 2001. In-flight calibration methods used for the Ørsted mission. In: *Ground and In-Flight Space Magnetometer Calibration Techniques, ESA SP-490* (eds A. Balogh and F. Primdahl).

Pedersen L.B. and Rasmussen T.M. 1990. The gradient tensor of potential field anomalies: Some implications on data collection and data processing of maps. *Geophysics* **55**, 1558–1566.

Primdahl F. 1979. The fluxgate magnetometer. *Journal of Physics E: Scientific Instruments* **12**, 241–253.

Sabaka T.J., Olsen N. and Purucker M.E. 2004. Extending comprehensive models of the Earth's magnetic field with Orsted and CHAMP data. *Geophysical Journal International* **159**, 521–547.

Schmidt P.W. and Clark D.A. 1998. The calculation of magnetic components and moments from TMI: A case study from the Kuckers igneous complex, Queensland. *Exploration Geophysics* **29**, 609–614.

Stolz R., Zakosarenko V., Schulz M., Chwala A., Fritzsch L., Meyer H.G. and Köstlin E.O. 2006. Magnetic full-tensor SQUID gradiometer system for geophysical applications. *The Leading Edge* **25**, 178–180.